minerals

MDPI

Article

Petrological, Geochemical and Chronological Characteristics of Dolomites in the Permian Maokou Formation and Constraints to the Reservoir Genesis, Central Sichuan Basin, China

Xuejing Bai [1,2], Jianfeng Zheng [2,3,*], Kun Dai [4,*], Shuxin Hong [1,2], Junmao Duan [2,3] and Yunmiao Liu [1,2]

1 Exploration and Development Research Institute, PetroChina Daqing Oilfield Co., Ltd., Daqing 163712, China; bxuejing@petrochina.com.cn (X.B.); hshuxin@petrochina.com.cn (S.H.); liuyunmiao@petrochina.com.cn (Y.L.)
2 Key Laboratory of Carbonate Reservoirs CNPC, Hangzhou 310023, China; duanjm_hz@petrochina.com.cn
3 PetroChina Hangzhou Research Institute of Geology, Hangzhou 310023, China
4 School of Earth Sciences, China University of Petroleum (Beijing), Beijing 102249, China
* Correspondence: zhengjf_hz@petrochina.com.cn (J.Z.); thous_nite@foxmail.com (K.D.)

Abstract: The Middle Permian Maokou Formation in the Sichuan Basin has huge resources and is an important target for natural gas exploration. In recent years, significant exploration breakthroughs have been made in the dolomite field of member Mao-2 in central Sichuan, and the gas production of several wells has exceeded 1×10^6 m^3/d, indicating promising prospects for exploration. However, the origin of the dolomite reservoir in member Mao-2 remains ambiguous, which restricts the accurate prediction of favorable reservoirs. This study focuses on drilling in the Hechuan area as its research object, by using a detailed description of the cores from member Mao-2 of seven wells; samples were selected for tests of the degree of dolomite cation ordering, stable carbon and oxygen isotopic compositions, strontium isotopic composition, rare earth elements, LA-ICP-MS element mapping and U-Pb dating. It is clarified that: (1) The crystalline dolomite of member Mao-2 in the Hechuan area is the main reservoir rock, and the heterogeneous vugs and fractures are the main reservoir space. The dolomite in member Mao-2 has been characterized by a low degree of cation ordering value (avg. 0.59), with values of $\delta^{13}C$ (avg. 3.87‰), $\delta^{18}O$ (avg. −7.15‰) and $^{87}Sr/^{86}Sr$ (avg. 0.707474) having similar geochemical characteristics to Middle Permian seawater; the REEs normalized distribution patterns have similar characteristics to limestone; and the U-Pb age (261.0~262.0 Ma) corresponds to the age in the Capitanian stage of the Permian Guadalupian Series. (2) Petrological studies show that member Mao-2 has vertical karstification zonation characteristics; syngenetic karstification controls the formation of a large-scale fracture-cave system in the phreatic zone; the dolomitization of sediment in the fracture-cave system occurred during the penecontemporaneous period with locally restricted seawater. (3) The main controlling factors of the reservoir were syngenetic karstification, early dolomitization and hydrothermal dissolution related to Emei taphrogenesis. The research results are of great significance for dolomite reservoir prediction; the highlands of paleogeomorphology with syndepositional faults are favorable areas for dolomite reservoirs.

Keywords: dolomite; geochemistry; chronology; reservoir genesis; Permian Maokou Formation; central Sichuan Basin

Citation: Bai, X.; Zheng, J.; Dai, K.; Hong, S.; Duan, J.; Liu, Y. Petrological, Geochemical and Chronological Characteristics of Dolomites in the Permian Maokou Formation and Constraints to the Reservoir Genesis, Central Sichuan Basin, China. *Minerals* **2023**, *13*, 1336. https://doi.org/10.3390/min13101336

Academic Editors: Hamzeh Mehrabi, Vahid Tavakoli and János Haas

Received: 15 August 2023
Revised: 2 October 2023
Accepted: 11 October 2023
Published: 17 October 2023

1. Introduction

Sichuan Basin is a large superposed petroliferous basin in southwest China [1]; its resources consist primarily of natural gas, with vast reserves, of which the total Permian resources are approximately 1.51×10^{12} m^3, with proven reserves of 881.3×10^8 m^3, and an exploration rate of only 5.84%, showing a great exploration potential. In the past two decades, significant progress has been made in the exploration of the Middle Permian Qixia Formation and Maokou Formation in northern and central Sichuan, with the discovery of the Yuanba, Shuangyushi and Moxi gas fields [2,3]; among these, the exploration of the

Maokou Formation has been targeting the top unconformable limestone karst reservoirs. In recent decades, great breakthroughs in the Maokou Formation of central Sichuan have been successful in obtaining economically viable gas flow from wells NC1, MX39 and JT1, sequentially [4], among which the gas production in well JT1 is 112.8 $\times$ 10^4 m^3/d [5], making this one of the important areas of risk exploration in Sichuan Basin. The previous three years, with the continuous high production of economically viable gas flow obtained from well HS4 (test gas production 113 $\times$ 10^4 m^3/d), TS4 (205 $\times$ 10^4 m^3/d) and TS11 (233 $\times$ 10^4 m^3/d) in the Hechuan area of Maokou Formation in central Sichuan, have further revealed that this target is a good exploration prospect.

The dolomite reservoir of the Middle Permian Maokou Formation has gradually become a research hotspot, with the continuous discovery of topics for exploration. Previous studies on dolomite reservoirs have mainly focused on dolomitization models, including seepage reflux, sabkha, burial dolomitization and hydrothermal dolomitization. For the origin of the dolomite, through the study of drilling and outcrops in the central Sichuan area, Liu's [6] research indicates that the insufficient mantle-derived hydrothermal fluids mixed with the fluids in the early fracture-cave system, resulting in dolomitization of the surrounding rocks. According to Jiang's [7] research on drilling cores in central Sichuan, the dolomite is originated by structural hydrothermal. Liu [8], based on the research of the drilling core from central Sichuan, thinks that the dolomite originated from the mixing of residual seawater in the strata and hydrothermal fluids associated with magma activity. As for the main controlling factors of dolomite reservoir genesis, Hu's [9] studies show that the dolomite reservoir in southwest Sichuan and central Sichuan is dominated by vuggy porosity; the main controlling factors of the reservoir are granular beach facies, epidiagenetic dissolution and buried hydrothermal dissolution. Hu [10] thought that, in the east Sichuan region, the dolomite reservoir is porous and fractured; the bioclastic beach, formation water subjected to magmatism and basement faults commonly control the genesis of reservoirs. The study of the Huaying Mountain outcrop area in eastern Sichuan by Li [11] shows that the dolomite reservoir is dominated by cracks and vuggy porosity, and the bioclastic beach and syndepositional faults are identified as the main factors controlling the genesis of reservoirs. However, it still fails to reach a consensus on the genesis of the dolomite reservoir of the Maokou Formation in the central Sichuan area. In addition, the lack of drilling data leads to difficulties in the prediction of favorable dolomite reservoirs. Therefore, the study of the diagenesis and genetics of dolomites is essential, to better deal with effective reservoir prediction and further exploration deployment in this area.

This paper discusses the genesis of the dolomite and the reservoir control factors in the Maokou Formation in the Hechuan area of the central Sichuan Basin, by using the cores of seven wells, through description and thin-section observations, tests of degree of dolomite cation ordering, stable carbon and oxygen isotopic compositions, strontium isotopic composition, rare earth elements, laser-ablation inductively-coupled-plasma mass spectrometry (LA-ICP-MS) element mapping, and U-Pb dating, so as to explore the genesis of the dolomite and the main factors controlling the reservoirs in the Maokou Formation, and thus identify the genesis and distribution of reservoirs in the Maokou Formation. The research findings provided effective guidance for the prediction of dolomite reservoir distribution in the Maokou Formation Hechuan Block, and are of great significance for dolomite reservoir evaluation for exploration in the central Sichuan Basin and even the entire basin.

2. Geological Setting

The Sichuan Basin is located in the eastern part of Sichuan Province, China (Figure 1a); it is a large superposed oil and gas basin developed on the basis of craton [12], with an area of about 19 $\times$ 10^4 km^2, the basin can be divided into five structural units: the north Sichuan low-steep structural belt, west Sichuan low-steep structural belt, south Sichuan low-steep structural belt, central Sichuan gentle structural belt and east Sichuan high-steep structural belt (Figure 1b). The Neoproterozoic to Middle Triassic basin evolution was

influenced by the extension-convergence cycles of the Rodinia and Pangaea continents, and it experienced four tectonic cycles [13]: the Yangtze cycle, Caledonian cycle, Hercynian cycle and Indochina cycle. Under the influence of the "Guangxi Movement" in the late Caledonian period, the Leshan-Longnusi paleo-uplift was formed, which placed the tectonic slope break belt on the periphery of the uplift depression of central and northern Sichuan in the highland of paleogeomorphology for a long time, and controlled the sedimentary pattern of the Early Permian [14,15]; and the "Dongwu Movement" in the late Middle Permian (sedimentary period of Maokou Formation) caused the tectonic differentiation of the basin [16]. It strongly promoted the maturity of the Lower Paleozoic to Lower Permian source rocks and the generation of oil and gas [17]. Emei taphrogenesis entered a high-incidence period, under a background of extensional and tensile gravity; the basement fault in the basin was revived, more tensile fractures were formed, and a series of NW-SE trending platform internal taphrogeneses were developed. At this time, the mantle plume uplifted in the Emeishan large igneous province (ELIP), resulting in the overall uplift of the Upper Yangtze region and large-scale uplift and denudation of the Maokou Formation in the basin. With the increase of mantle plume uplift in the later period, rapid subsidence occurred in the central and northern parts of the basin, while the southwest inherited higher paleogeomorphological characteristics, providing conditions for the karst at the top of the Maokou Formation [18,19].

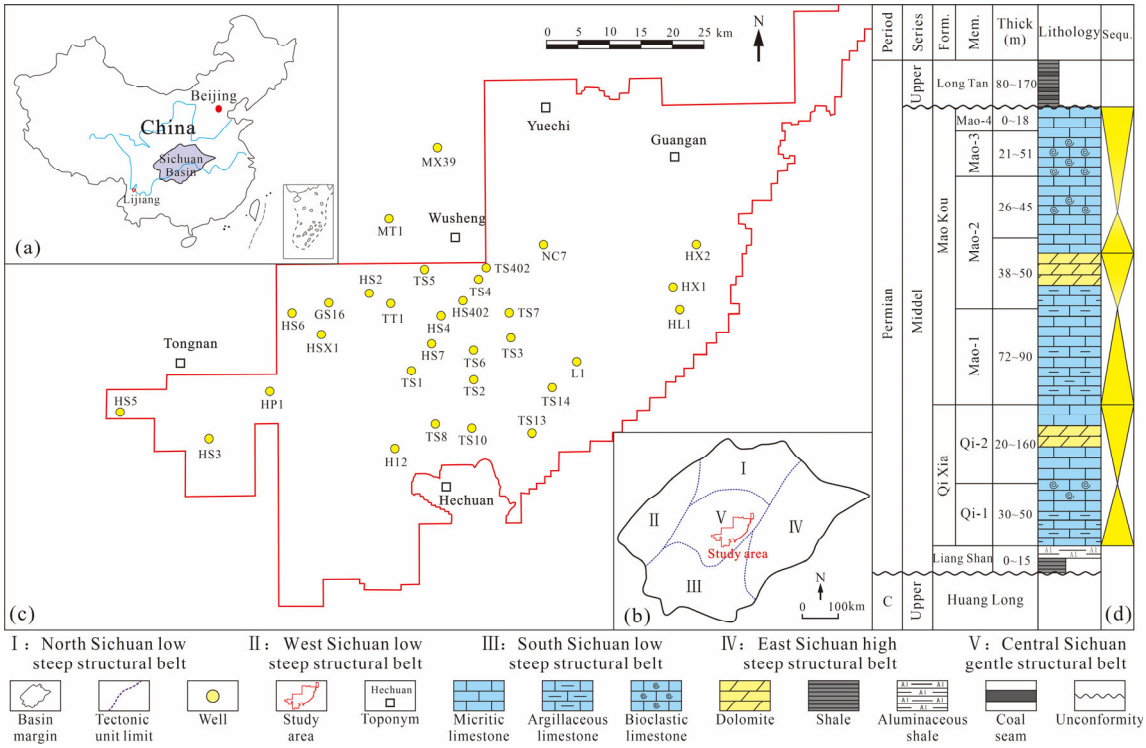

Figure 1. Geological setting map of the study area: (**a**) Location of the Sichuan Basin in eastern Sichuan Province, China is shown in the purple zone; (**b**) Tectonic location of the study area indicated with a red line polygon; (**c**) Well location in the study area; (**d**) Stratigraphic sequence of Middle Permian Maokou Formation.

The Hechuan area belongs to the gentle structural belt in central Sichuan (Figure 1b,c), which experienced a gradual transition from clastic rock deposition to carbonate rock deposition in the Middle Permian, and developed the Liangshan Formation, Qixia Formation and Maokou Formation (Figure 1d) from bottom to top. The Liangshan Formation was in parallel unconformable contact with the Carboniferous strata. In the early Middle Permian, there was extensive transgression in the Sichuan Basin, and the Liangshan Formation mainly developed shore swamp facies of sandy mudstone [20]; with a step of transgression,

the study area gradually evolved into a carbonate gentle slope sedimentary system. The Qixia Formation is composed of a third-order sequence; during the transgression period of the Qixia Formation, it mainly developed medium gentle slope argillaceous limestone and wackestone; in the highstand, inner gentle slope facies of packstone, grainstone and crystalline dolomite are mainly developed. The Maokou Formation is composed of two third-order sequences, which can be divided into four members from bottom to top: Mao-1, Mao-2, Mao-3, and Mao-4. The member Mao-1 has the structural characteristics of "eyelid and eyeball" (Figure 2a,b), with a thickness of about 72 m to 90 m. The "eyelid limestone" is mainly dark gray-black argillaceous limestone with high organic matter content, and the "eyeball limestone" is mainly wackestone/packstone [21]. The member Mao-2 mainly develops dark gray layered argillaceous limestone, gray wackestone/packstone (Figure 2c) and dark gray dolomite/dolomite with limestone (Figure 2d); it contains a lot of foraminifers, green algae, coral, brachiopods and other biological debris, with an overall thickness of about 60~90 m. Among these, dolomite is distributed in the lower middle part of member Mao-2, which is relatively continuous horizontally, but the thickness varies greatly (2~22 m). The dolomite crystals are mainly fine-grained to medium-finely crystalline dolomite (Figure 2e). The restoration of the dolomite protolith structure shows that the protolith of crystalline dolomite is bioclastic limestone (Figure 2f,g); member Mao-3 is 26–45 m thick, mainly developed with gray bioclastic packstone; member Mao-4 is generally absent, and mainly develops dark gray bioclastic packstone, which is in parallel unconformity with the overlying Longtan Formation (Figure 1d).

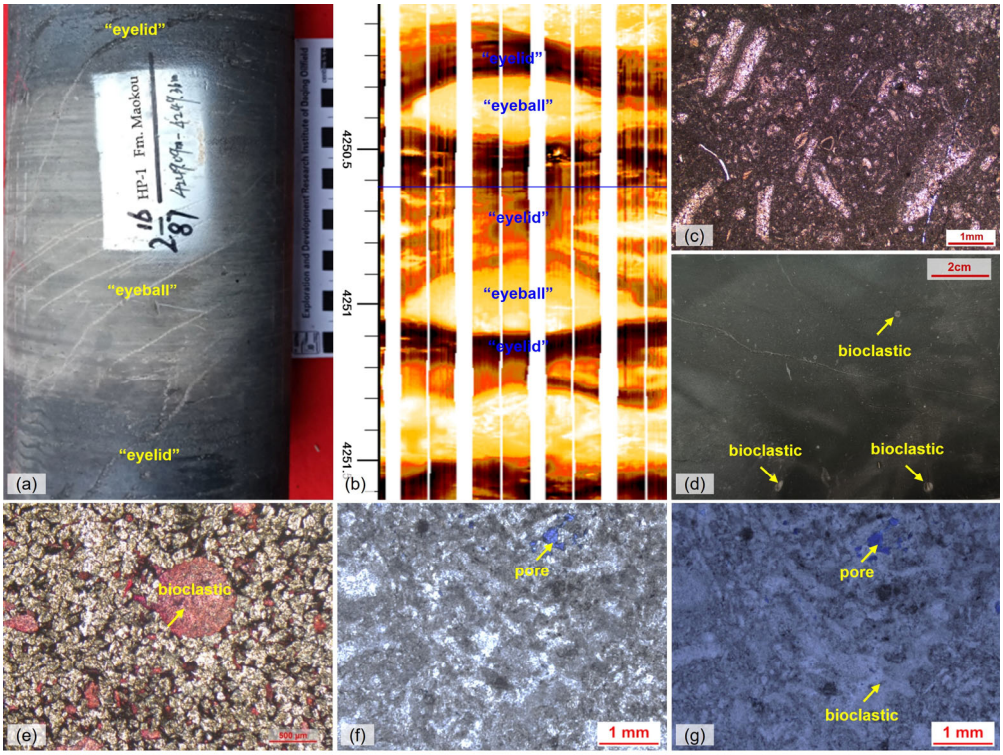

Figure 2. Photographs of carbonate rocks in the Maokou Formation: (**a**) "Eyeball-eyelid" structure, well HP1, member Maokou-1, core; (**b**) "Eyeball-eyelid" structure, well HP1, member Maokou-1, core; (**c**) Bioclastic limestone, well HS4, member Mao-2, thin section PPL image; (**d**) Dolomite with undolomitized bioclastics, well TS4, member Mao-2, slabbed coe; (**e**) Crystalline dolomite with alizarin red stain, the component stained red is calcite bioclastic, well HS4, member Mao-2, thin section PPL image; (**f**) Crystalline dolomite, well TS4, member Mao-2, thin section PPL image; (**g**) Same view as (**f**), the bioclastic profile is clear by protolith reconstruction, thin section PPL image.

3. Petrology

The member Mao-2 dolomite development in the Hechuan area has zonation characteristics (Figure 3a). The dolomite is darker in color and develops fractures filled with saddle-shaped dolomite (Figure 3b), gray irregularly rounded limestone "breccia" commonly in the upper and lower of the dark gray dolomite zone (Figure 3c); near the top and bottom of the dolomite zone is a dolomitic limestone zone. Dark gray dolomite has the characteristics of "groove" distribution, which "cuts" the gray limestone into a "breccia" (Figure 2d). A dark gray "network" calcareous dolomite can be found in the gray limestone zone (Figure 2e). Overall, the dolomite and limestone boundaries of member Mao-2 are clear and can be recognized with the naked eye.

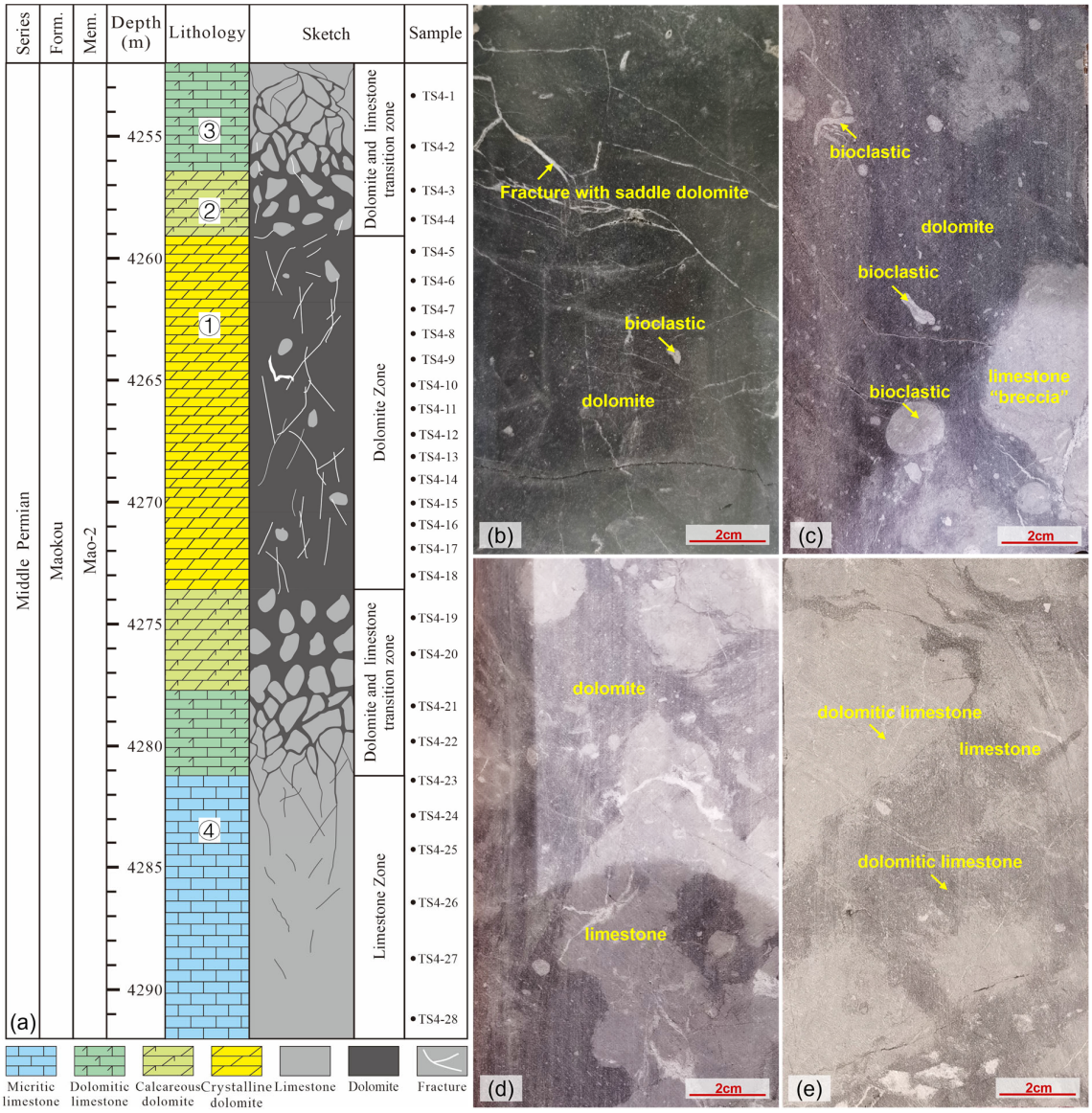

Figure 3. Core characteristics of member Mao-2 in well TS4: (**a**) Core column; (**b**) Photograph of position ① in dolomite zone; (**c**) Photograph of position ② in dolomite and limestone transition zone; (**d**) Photograph of position ③ in dolomite and limestone transition zone; (**e**) Photograph of position ④ in limestone.

Pores are found almost exclusively in the dolomite of member Mao-2; the types of pores include vugs (Figure 4a,b), intercrystalline (dissolved) pores (Figure 4c,d), and fractures (Figure 4e,f), among which vugs are the most common and are mainly distributed

unevenly along the fractures (Figure 4b,h). White saddle dolomite is the most common in the vugs and fractures (Figure 4b,f–k), which has the characteristics of undulatory extinction under the microscope (Figure 4i), and asphalt (Figure 4j,k) is common above the saddle dolomite. In addition, the vugs were filled with quartz, fluorite (Figure 4k) and sparry calcite (Figure 4j,k). In conclusion, the vugs and fractures are usually filled with one or more minerals; the whole is characterized by sequentially cemented saddle dolomite-pitch-quartz/fluorite-calcite from the edge of the vug to the center.

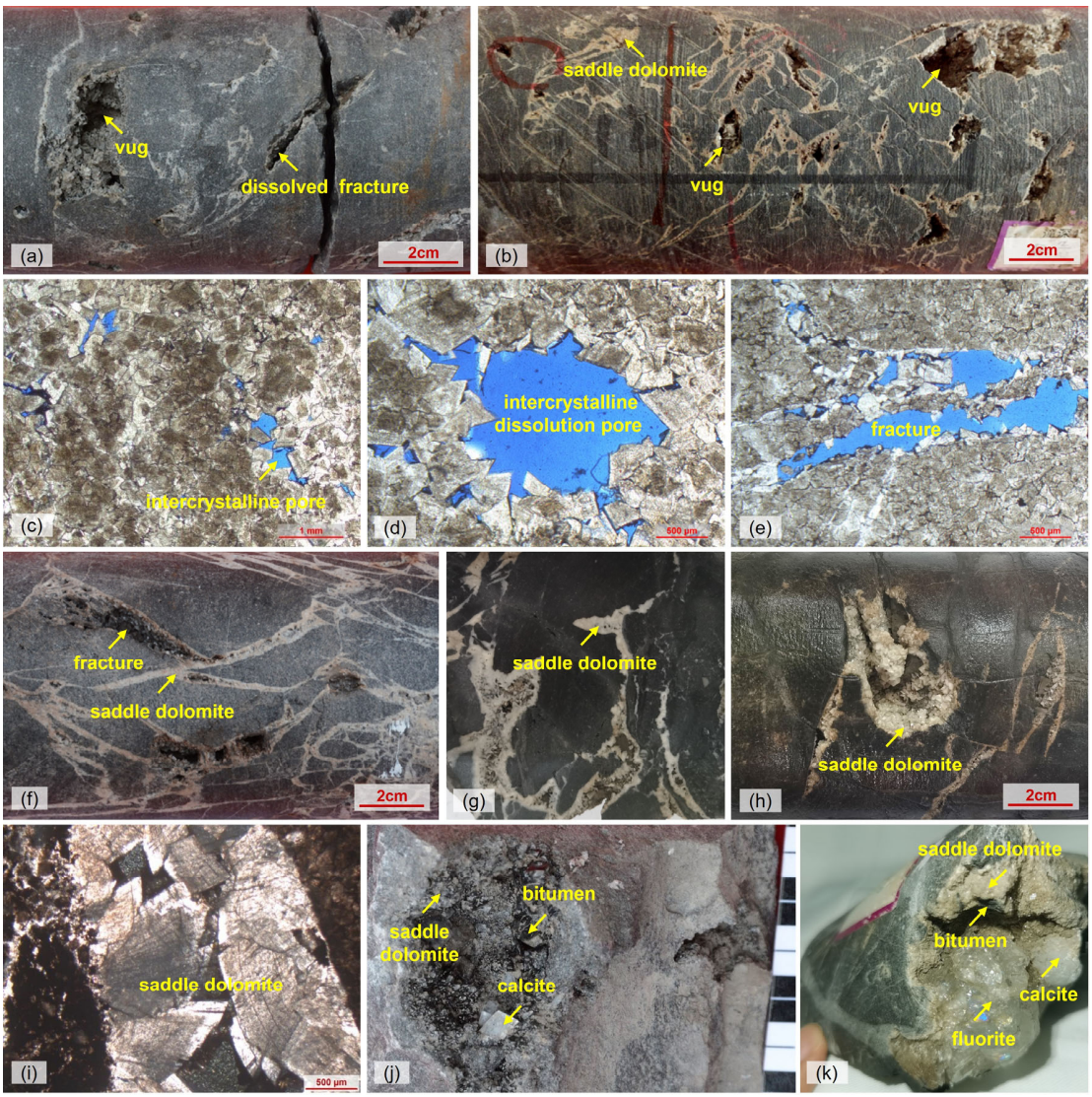

Figure 4. Photographs of dolomite reservoir in the Maokou Formation: (**a**) Dolomite with vugs and dissolved fractures, well TS402, member Mao-2, core; (**b**) Dolomite with vugs and fractures, the rock broke up and became brecciated, well TS4, member Mao-2, core; (**c**) Mesocrystalline dolomite with pores, well TS3, member Mao-2, blue casting thin section PPL image; (**d**) Mesocrystalline dolomite with pores, well TS3, member Mao-2, blue casting thin section PPL image; (**e**) Mesocrystalline dolomite with pores, well HS3, member Mao-2, blue casting thin section PPL image; (**f**) Dolomite with fractures, well HS402, member Mao-2, core; (**g**) Dolomite with fractures, well TS4, member Mao-2, core; (**h**) Dolomite with vugs and fractures, well TS4, member Mao-2, core; (**i**) Saddle dolomite in the fracture, well TS4, member Mao-2, thin section XPL image; (**j**) Dolomite with vugs, the vugs are filled with saddle dolomite, bitumen and sparry calcite, well TS402, member Mao-2, core; (**k**) Dolomite with vugs, the vugs are filled with saddle dolomite, bitumen, fluorite and sparry calcite, well TS13, member Mao-2, core.

4. Samples and Methods

A total of 38 carbonate rock samples were collected through research, all of which came from the Maokou Formation of TS4 Well in the Hechuan area, Sichuan Basin. Member Mao-2 of the Maokou Formation of this well encountered dolomite of about 22 m, which is the well with the largest thickness of dolomite in the study area. All samples were made into cast thin sections. Based on core characteristics and thin-section microscopy analysis, 28 dolomite samples were selected for whole-rock carbon and oxygen isotopes ($\delta^{13}C$ and $\delta^{18}O$), 19 samples for strontium isotopes, 14 samples for dolomite ordering, and 16 samples for rare earth element detection and analysis. In order to minimize the interaction between carbonate cements and host rocks, single structural components were drilled from all samples using a small micro-sampling drill, ground to a powder of 200 mesh with an agate marl. Then, the sample powder was packaged with transparent drawing paper. In addition, 1 sample was selected for elemental mapping (Figure 5a; Table 1), and 3 samples for laser U-Pb dating detection (Figure 5b–d). Before the LA-ICP-MS trace elemental mapping and laser U-Pb dating detection, the samples were made into a 100 µm thick sections, and then polished on a single side, and purified in a super-clean laboratory.

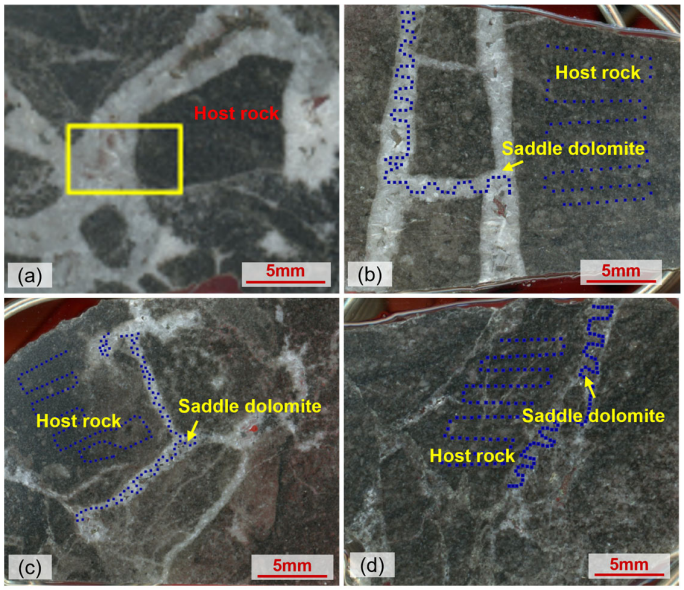

Figure 5. Photographs of the Maokou Formation test sample ((**a**) is an elemental mapping sample, where the yellow rectangle is element mapping area; (**b**–**d**) are U-Pb dating samples): (**a**) sample TS4-8; (**b**) Sample TS4-6; (**c**) Sample TS4-10; (**d**) Sample TS4-17.

Table 1. Message of the sample.

Lithology	Member	Sample	Depth/m	Lithology	Member	Sample	Depth/m
Limestone	Mao-2	TS4-1	4253.3	Dolomite	Mao-2	TS4-15	4270
Limestone	Mao-2	TS4-2	4255.4	Dolomite	Mao-2	TS4-16	4270.9
Dolomite	Mao-2	TS4-3	4257.2	Dolomite	Mao-2	TS4-17	4271.9
Dolomite	Mao-2	TS4-4	4258.4	Dolomite	Mao-2	TS4-18	4273
Dolomite	Mao-2	TS4-5	4259.7	Dolomite	Mao-2	TS4-19	4274.7
Dolomite	Mao-2	TS4-6	4260.9	Limestone	Mao-2	TS4-20	4276.2
Dolomite	Mao-2	TS4-7	4262.1	Limestone	Mao-2	TS4-21	4278.4
Dolomite	Mao-2	TS4-8	4263.1	Limestone	Mao-2	TS4-22	4279.8
Dolomite	Mao-2	TS4-9	4264.2	Limestone	Mao-2	TS4-23	4281.4

Table 1. *Cont.*

Lithology	Member	Sample	Depth/m	Lithology	Member	Sample	Depth/m
Dolomite	Mao-2	TS4-10	4265.2	Limestone	Mao-2	TS4-24	4282.8
Dolomite	Mao-2	TS4-11	4266.2	Limestone	Mao-2	TS4-25	4284.3
Dolomite	Mao-2	TS4-12	4267.2	Limestone	Mao-2	TS4-26	4286.4
Dolomite	Mao-2	TS4-13	4268.1	Limestone	Mao-2	TS4-27	4288.7
Dolomite	Mao-2	TS4-14	4269.1	Limestone	Mao-2	TS4-28	4291.2

Determination of the order degree of dolomite, and whole-rock C, O and Sr isotope measurement, REEs and LA-ICP-MS trace elemental mapping and U-Pb dating, were all completed in the Key Laboratory of Carbonate rock Reservoir of CNPC (Hangzhou). Order degree of dolomite was measured using an X′pert Pro X-ray diffractometer, with a relative error <10%; the X-ray diffraction peak ratio (015)/(110) was used to calculate the order degree [22]. The whole-rock C and O isotope detection instrument was a Delta V Advantage isotope ratio mass spectrometer. GBW4405 and GBW4406 standard samples were used in the test process. The test results were standardized using the Cretaceous Vienna PeeDee Belemnite (VPDB) [23]. The test accuracy of $\delta^{13}C$ is ±0.06‰ and the test accuracy of $\delta^{18}O$ is ±0.08‰. Whole-rock Sr isotope measurement was conducted with a Triton Plus IRMS (Isotope Ratio Mass Spectrometry), when the carbonate standard reference material of GBW04411 was used, and a precision better than 0.01% was obtained. The REEs detection instrument model was a Thermo iCAP TQ ICP-MS. W-2a and BHVO-2 international standard samples were used in the test process, and the analysis accuracy and accuracy are better than 5%. LA-ICP-MS trace elemental mapping used an ASI RESOlution LR laser ablation system; erosion using square beam spot is 40 microns in length, beam spot movement rate 0.04 mm/s. The test instrument model was a Thermo iCAP TQ ICP-MS; an NIST612 standard sample was used in the test process, original data were processed by Iolite 3.6 (University of Melbourne, Parkville, VIC, Australia) to generate element distribution images. Laser U-Pb dating detection used a COHERENT GeoLasHD laser ablation system, denudation is 160 microns in diameter circular beam spot. The test instrument model was an Element XR ICP-MS. Two international standard samples, NIST614 and WC-1, and DaMY-1 laboratory standard samples were used in the test process [24]. After the data were processed by Iolite3.6, Isoplot3.0 (University of California Berkeley, Berkeley, CA, USA) was used to calculate the age and draw the Tera-Wasserburg concordia diagram.

5. Results

5.1. Degree of Dolomite Cation Ordering

Dolomite is a tripartite crystal system mineral, and its lattice parameters are affected by composition, temperature and pressure [25]; the ideal crystal structure of dolomite is where Ca^{2+} and Mg^{2+} are arranged alternately along the c axis, and the molar percentage of Ca^{2+} and Mg^{2+} is the same, but in disordered dolomite, Ca^{2+} and Mg^{2+} are randomly distributed, similar to the structure of calcite. The degree of dolomite cation ordering is an important index for measuring the crystallization speed, crystallization temperature and evolution degree of dolomite; the slower the crystallization speed and the higher the crystallization temperature, the higher the degree of dolomite cation ordering, and vice versa [26]. In general, the degree of dolomite cation ordering greater than 0.8 is defined as high order, 0.6~0.8 is defined as secondary order, 0.4~0.6 is defined as low order, and less than 0.4 is defined as disorder [27]. According to the test results of 14 dolomite samples (Table 2), the dolomite degree of dolomite cation ordering of member Mao-2 of the TS4 well in the Hexhuan area ranges from 0.51 to 0.71, with an average value of 0.59, which belongs to the low order degree.

Table 2. Order degree, $\delta^{13}C$, $\delta^{18}O$ and $^{87}Sr/^{86}Sr$ values of dolomite (whole rock) in the Maokou Formation.

Sample	Lithology	Order Degree	$\delta^{13}C$ ‰ (PDB)	$\delta^{18}O$ ‰ (PDB)	$^{87}Sr/^{86}Sr$
TS4-1	Limestone	/	4.54	−7.03	0.707266
TS4-2	Limestone	/	4.30	−7.31	/
TS4-21	Limestone	/	4.28	−7.45	0.707317
TS4-22	Limestone	/	4.14	−6.82	/
TS4-23	Limestone	/	4.61	−7.27	0.707223
TS4-24	Limestone	/	4.01	−6.94	/
TS4-25	Limestone	/	4.46	−7.59	0.707215
TS4-26	Limestone	/	4.65	−6.94	0.707330
TS4-27	Limestone	/	4.17	−7.64	/
TS4-28	Limestone	/	4.25	−6.95	0.707245
TS4-3	Dolomite	0.58	3.93	−7.62	0.707278
TS4-4	Dolomite	0.55	3.98	−6.74	0.707341
TS4-5	Dolomite	0.54	3.77	−7.19	0.707452
TS4-6	Dolomite	0.69	4.09	−7.33	/
TS4-7	Dolomite	0.71	3.90	−7.57	0.707380
TS4-8	Dolomite	0.59	3.93	−6.94	0.707415
TS4-9	Dolomite	/	3.82	−7.48	/
TS4-10	Dolomite	0.60	3.80	−7.25	0.707324
TS4-11	Dolomite	/	4.03	−6.79	/
TS4-12	Dolomite	0.59	3.63	−6.71	0.707458
TS4-13	Dolomite	/	4.07	−6.84	/
TS4-14	Dolomite	0.55	3.93	−6.73	0.707497
TS4-15	Dolomite	0.63	3.78	−7.00	0.707593
TS4-16	Dolomite	0.51	3.95	−7.46	0.707676
TS4-17	Dolomite	/	3.71	−7.03	0.707639
TS4-18	Dolomite	0.56	3.76	−7.41	/
TS4-19	Dolomite	0.60	3.52	−7.55	0.707587
TS4-20	Dolomite	0.60	4.03	−7.07	0.707533

5.2. Stable Carbon and Oxygen Isotopic Compositions

Stable carbon and oxygen isotopic compositions of dolomitization are related to the stable carbon and oxygen isotopic compositions of dolomitization objects and the fluids that cause dolomitization, and are mainly affected by the salinity and temperature of the fluids [28]. Generally, the carbon and oxygen isotopes of sea water migrate in a positive direction due to evaporation, while the oxygen isotopes of underground brine will migrate in a negative direction due to high temperatures under buried conditions [29]. According to the whole-rock carbon and oxygen isotope test results of 28 carbonate samples (10 limestone samples, 18 dolomite samples) from member Mao-2 of well TS4 in the Hechuan area (Table 2) and the binary scatter diagram (Figure 6), there is no obvious correlation between $\delta^{13}C$ and $\delta^{18}O$ values, indicating that the samples are weakly affected by late diagenetic transformation. The basic information on diagenetic fluid is basically preserved. The $\delta^{13}C$ and $\delta^{18}O$ values of the dolomite range from 3.52‰ to 4.09‰ and −7.64‰ to −6.71‰, respectively, with average values of 3.87‰ and −7.15‰, the $\delta^{13}C$

and $\delta^{18}O$ values of the limestone range from 4.01‰ to 4.65‰ and −7.64‰ to −6.82‰, respectively, with average values of 4.34‰ and −7.19‰.

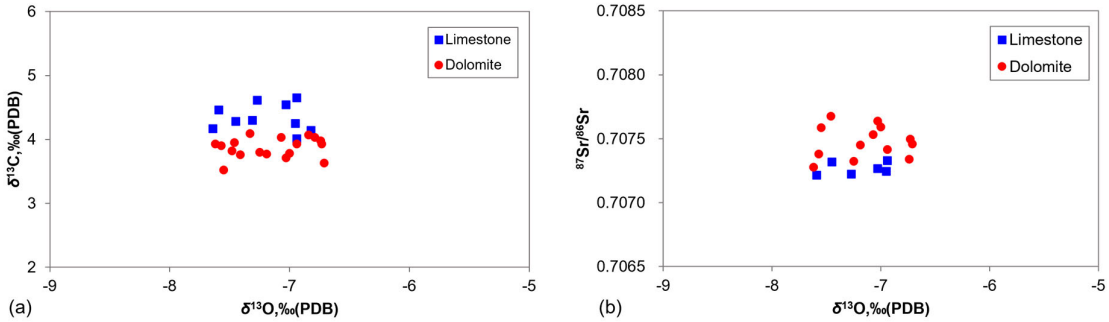

Figure 6. Binary plots of geochemistry of carbonate rocks of member Mao-2; (**a**) $\delta^{13}C$ versus $\delta^{18}O$; (**b**) $^{87}Sr/^{86}Sr$ versus $\delta^{18}O$.

5.3. Stable Strontium Isotopic Composition

Stable strontium isotopes are important parameters indicating paleoclimate and diagenetic fluid properties [30]. According to the whole-rock strontium isotope test results (Table 2) and the $^{87}Sr/^{86}Sr$ and $\delta^{18}O$ binary scatter diagram (Figure 6) of 19 carbonate samples from the TS4 well of member Mao-2, Hexhuan area, it can be seen that the $^{87}Sr/^{86}Sr$ value of dolomite ranges from 0.707278 to 0.707676; the average value is 0.707474. The $^{87}Sr/^{86}Sr$ values of limestone range from 0.707215 to 0.707330, and the average value is 0.707266. Overall, the 87Sr/86Sr value of dolomite is slightly higher than that of limestone, which conforms to the general law that the 87Sr/86Sr value of dolomite samples is usually higher than that of limestone samples [31].

5.4. Rare Earth Elements

The relative abundance of rare earth elements in carbonate minerals mainly depends on the content of rare earth elements in the fluid [32]. Rare earth elements enter the carbonate framework mainly through Ca^{2+} of metasomatic carbonate minerals, and their content is very weakly affected during the diagenetic process. Therefore, it can better indicate the sedimentary environment and the source of dolomitization fluid [33]. According to the rare earth element test results of 13 carbonate samples from the TS4 well of member Mao-2 in the Hechuan area (Table 3), ΣREEs of dolomite ranges from 1.284 ppm to 4.168 ppm, with an average value of 2.9 ppm. The ΣREEs of limestone ranges from 0.917 ppm to 1.822 ppm, with an average value of 1.37 ppm. In general, dolomite ΣREEs are higher than limestone. The measured results were standardized for the Australian Post-Archean mean shale (PAAS) [34], and the standardized (SN) element anomalies were calculated using the following methods: $\delta Ce = 2 \times Ce_{SN}/(La_{SN} + Pr_{SN})$, $\delta Eu = 2 \times Eu_{SN}/(Sm_{SN}+)$ [25]; if δCe and δEu are greater than 1.2, they are judged as positive anomalies; if δEu and δCe are less than 0.8, they are judged as negative anomalies. As can be seen from the standardized rare earth element partitioning pattern (Figure 7), both dolomites and limestone have the characteristics that the content of light rare earth elements (La~Eu) is smaller than that of heavy rare earth elements (Gd~Lu), showing no "tilt upward" pattern. There are no δCe and δEu anomalies in dolomite and limestone, but there is a positive δEu anomaly in one dolomite sample.

Table 3. Rare earth elements content values of dolomite in member Mao-2.

Sample	Lithology	La (ppm)	Ce (ppm)	Pr (ppm)	Nd (ppm)	Sm (ppm)	Eu (ppm)	Gd (ppm)	Tb (ppm)	Dy (ppm)	Ho (ppm)	Er (ppm)	Tm (ppm)	Yb (ppm)	Lu (ppm)	ΣREEs (ppm)
TS4-1	Limestone	0.277	0.494	0.059	0.227	0.042	0.009	0.045	0.007	0.045	0.011	0.034	0.005	0.034	0.005	1.294
TS4-22	Limestone	0.195	0.358	0.041	0.158	0.031	0.006	0.031	0.005	0.032	0.007	0.024	0.004	0.022	0.003	0.917
TS4-25	Limestone	0.375	0.692	0.083	0.32	0.066	0.013	0.068	0.011	0.068	0.016	0.049	0.008	0.046	0.007	1.822

Table 3. *Cont.*

Sample	Lithology	La (ppm)	Ce (ppm)	Pr (ppm)	Nd (ppm)	Sm (ppm)	Eu (ppm)	Gd (ppm)	Tb (ppm)	Dy (ppm)	Ho (ppm)	Er (ppm)	Tm (ppm)	Yb (ppm)	Lu (ppm)	ΣREEs (ppm)
TS4-27	Limestone	0.324	0.526	0.066	0.257	0.052	0.01	0.056	0.009	0.058	0.014	0.043	0.006	0.035	0.006	1.462
TS4-4	Dolomite	0.489	0.903	0.107	0.395	0.076	0.014	0.074	0.012	0.08	0.018	0.055	0.008	0.053	0.009	2.293
TS4-6	Dolomite	0.346	0.633	0.077	0.285	0.06	0.011	0.065	0.01	0.066	0.015	0.048	0.007	0.044	0.007	1.674
TS4-7	Dolomite	0.554	1.030	0.123	0.461	0.089	0.016	0.089	0.014	0.086	0.021	0.065	0.011	0.067	0.01	2.636
TS4-8	Dolomite	0.828	1.570	0.177	0.651	0.128	0.025	0.122	0.02	0.128	0.030	0.084	0.013	0.079	0.013	3.868
TS4-9	Dolomite	0.705	1.390	0.166	0.638	0.138	0.026	0.135	0.022	0.138	0.032	0.097	0.016	0.095	0.015	3.613
TS4-10	Dolomite	0.751	1.413	0.166	0.617	0.12	0.021	0.115	0.018	0.117	0.027	0.083	0.013	0.082	0.013	3.556
TS4-11	Dolomite	0.871	1.640	0.198	0.739	0.142	0.024	0.134	0.021	0.138	0.031	0.1	0.016	0.098	0.016	4.168
TS4-12	Dolomite	0.651	1.178	0.140	0.521	0.101	0.019	0.098	0.016	0.100	0.023	0.071	0.011	0.068	0.011	3.008
TS4-14	Dolomite	0.270	0.471	0.060	0.234	0.046	0.012	0.048	0.008	0.049	0.012	0.034	0.005	0.030	0.005	1.284

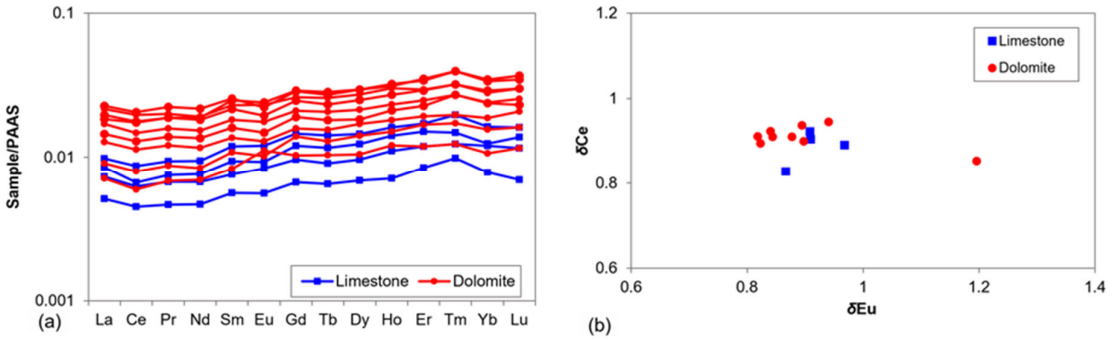

Figure 7. Rare earth element map of carbonate rocks of member Mao-2 in Hechuan area: (**a**) REEs normalized distribution patterns; (**b**) REEs binary plots of geochemistry: δCe versus δEu.

5.5. Element Mapping

The element composition of multi-phase cements in carbonate fractures and vugs is non-uniform. Element mapping technology based on LA-ICP-MS is used to directly display the characteristics of the element plane changes in the millimeter–centimeter region of the sample, which is helpful for analyzing the origin of the sub-cements of different periods [35]. The plane distribution characteristics of Mg and Ca can judge the type of mineral. Trace elements Mn, Fe, Sr, Ba, Th, U and rare earth elements Y, La, Ce, Eu are relatively sensitive to the characteristics of diagenetic fluid, and the source and environment of diagenetic fluid can be analyzed according to their plane distribution characteristics [27].

According to the element mapping of sample TS4-8 (Figure 8), the area (red) with high and uniform distribution of major elements Mg and Ca is dolomite, while the area (black) without Mg and Ca is noncarbonate rock mineral. Combined with the rock characteristics in Figure 5a, it can be ascertained that the host rock is dolomite, and two phases of cements can be identified in the fracture: phase I is dolomite, which is symmetrically distributed along the edge of both sides of the fracture; phase II is quartz (judging by the absence of calcium in the mineral and the quartz seen in the core vugs and fractures). Based on the distribution characteristics of trace and rare earth elements, it can be seen that the host rock has high Sr, Ce, Y, Th, Fe, La, U and low Eu, Mn, Ba values. The host rock edge has higher Mn and lower Ce, Y, Th, Fe, La, U values, and almost no Ba element; there is a difference between them. The distribution of trace and rare earth elements in the host rock edge is similar to that of dolomite in phase I.

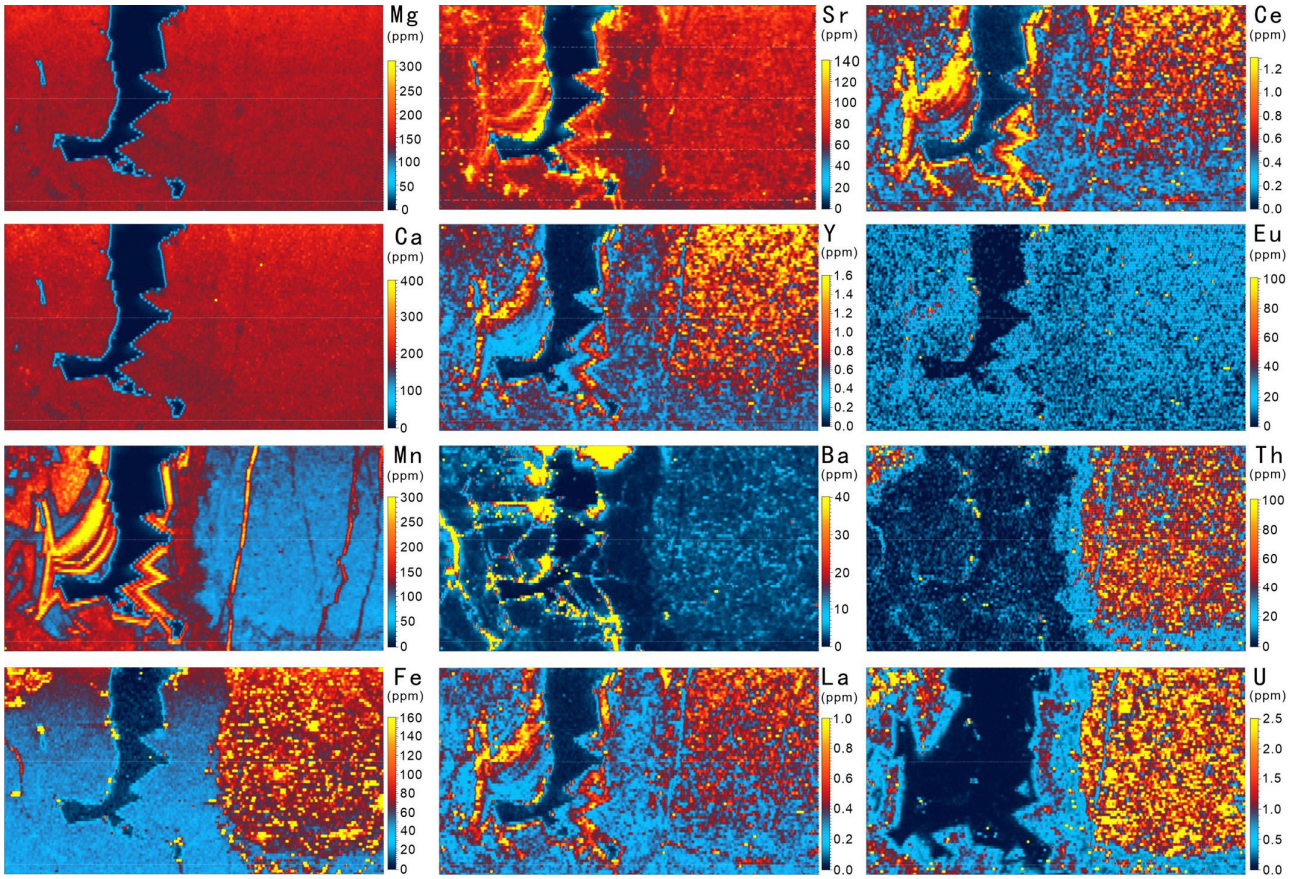

Figure 8. Element mapping based on LA-ICP-MS, sample TS4-8.

5.6. U-Pb Dating

An U-Pb dating technique of carbonate rocks based on LA-ICP-MS can be used to determine the relative diagenetic ages of carbonate minerals [24,36]. According to the test results (Table 4, Figure 9), the age of the host rock of sample TS4-6 is 261 ± 6.1 Ma with the MSWD (mean square of weighted deviates) value of 2.2, and the age of the saddle dolomite in the fracture is 256 ± 10 Ma with the MSWD value of13. The age of host rock of sample TS4-10 is 261.0 ± 4 Ma with the MSWD value of 2, and that of saddle dolomite in the fracture is 258.9 ± 5.1 Ma with the MSWD value of 7.1. The age of the host rock of sample TS4-15 is 262 ± 16 Ma with the MSWD value of 9.9, and the age of saddle dolomite in the fracture is 260 ± 2.4 Ma with the MSWD value of 3. It can be seen that the host rock of the three dolomite samples in member Mao-2 are similar in age, and the corresponding stratigraphic age is the Capitanian stage of the Permian Guadalupian Series (259.51~264.28 Ma). The age of saddle dolomite of the three samples is also close, and the corresponding stratigraphic age is from the Wuchiapingian stage to Changhsingian Stage (251.9~259.51 Ma) of the Permian Lopingian Series. In addition, the age of the host rock of the three samples is greater than that of the saddle dolomite in the fracture, which reveals that it is consistent with the rock sequence, and therefore reflects that the measurement results are relatively reliable.

Table 4. The result of U-Pb dating in member Mao-2 samples.

Sample	Components	U-Pb Age (Ma)	Components	U-Pb Age (Ma)
TS4-6	Host rock (dolomite)	261 ± 6.1	Saddle dolomite	256.0 ± 10

Table 4. *Cont.*

Sample	Components	U-Pb Age (Ma)	Components	U-Pb Age (Ma)
TS4-10	Host rock (dolomite)	261.0 ± 4.0	Saddle dolomite	258.9 ± 5.1
TS4-15	Host rock (dolomite)	262.0 ± 16	Saddle dolomite	260.0 ± 2.4

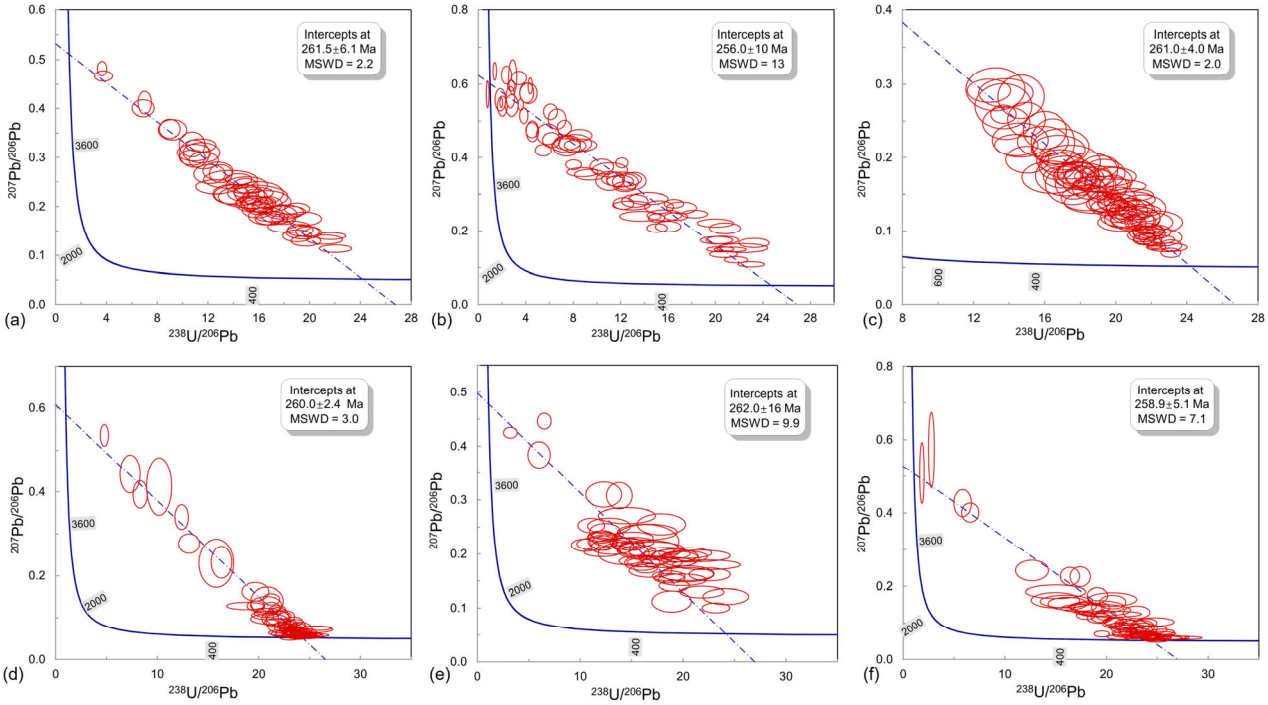

Figure 9. LA-ICP-MS U-Pb concordia diagram of dolomite in the Maokou Formation (The blue line represents the theoretical age curve when the sample U-Pb system is always closed. The blue dashed line represents the theoretical age curve with certain initial Pb in the sample U-Pb system, but it has been closed since its formation. The lower intersection point between the blue line and the sample U-Pb system is the rock formation age. The red circle represents the margin of error): (**a**) Host rock of sample TS4-6; (**b**) Saddle dolomite of sample TS4-6; (**c**) Host rock of sample TS4-10; (**d**) Saddle dolomite of sample TS4-10; (**e**) Host rock of sample TS4-15; (**f**) Saddle dolomite of sample TS4-15.

6. Discussion

6.1. Genesis of Dolomite

Dolomitization can improve the compressive properties of rocks; the dolomitization of the early diagenetic stage plays an important constructive role in the preservation of primary pores and early dissolved pores; however, dolomitization in the late burial stage had little effect on early pore preservation. In addition, large-scale pressure dissolution not only causes compaction of pore space, but also the calcium fluid which forms the pressure dissolution can fill primary pores. It has a destructive effect on the reservoir [37,38], so it is significant to judge the time of dolomitization.

According to the geochemical data obtained by analysis and testing, the $\delta^{13}C$ (avg. 3.87‰) and $\delta^{18}O$ (avg. 7.15‰) values of dolomite in member Mao-2 are within the variation range of seawater in the Middle Permian ($\delta^{18}O$ ranges from 7‰ to 4‰ and $\delta^{13}C$ ranges from 3‰ to 5‰) [30,39]. The range of $\delta^{18}O$ values of dolomite and limestone is similar, but the $\delta^{13}C$ of limestone is higher than that of dolomite, which is related to the rise and fall of sea levels. During the rise of sea levels, the rate of organic carbon burial increases, resulting in a corresponding increase in the $\delta^{13}C$ value of limestone, whereas a large amount

of ^{12}C enters the seawater during the fall of sea levels. The $\delta^{13}C$ value of the dolomite decreases during the same period [30]. The $^{87}Sr/^{86}Sr$ values (average 0.707474) are also close to the coeval seawater [30,39], indicating that the dolomitization fluid in member Mao-2 was seawater [40]. Dolomite and limestone in member Mao-2 have similar REEs normalized distribution patterns, which reveals that dolomite and limestone have similar diagenetic fluids (seawater). In addition, the low ΣREEs content of dolomite (avg. 2.9 ppm) and the unobvious overall anomalies of δCe and δEu also indicate that dolomite did not undergo transformation by meteoric water and hydrothermal fluid during diagenesis. Member Mao-2 has a low degree of dolomite cation ordering (avg. 0.59), indicating that the dolomitization process was characterized by rapid replacement and crystal growth. The U-Pb age (259.51~264.28 Ma) is within the age range of the Capitanian stage of the Permian Guadalupian Series, indicating that dolomite was formed in a penecontemporaneous period. In a word, member Mao-2 dolomites were formed in a penecontemporaneous period with seawater as the dolomitization fluid.

As mentioned above, the vertical karst zonation characteristics of member Mao-2 in the study area are displayed. The dark gray dolomite at the transition zone of dolomite and limestone is a "network of cut" limestone, which is "breccia" (Figure 4), the "brecciform" limestone without edges and corners, and the sedimentary particles in the "network" have the characteristics of a vadose zone, which is similar to the vertical vadose zone in a kast fracture-cave system. Below the transition zone of dolomite and limestone is the dolomite zone; it has irregular limestone "breccia" at the top and bottom, not touching, and a few isolated "breccia" in the middle; this zone has the same characteristics as a horizontal phreatic zone in kast. Below the dolomite zone is limestone with dolomitic, and the "network fracture" with dark grey gradually changes downward into a high angle "fracture" until it disappears. These characteristics indicating the fracture-cave system may develop in member Mao-2. In addition, from the geological background, there is a sequence boundary in member Mao-2 at the study area, which indicates that it had a long exposure and karstification during the sedimentary period [20]. According to the drilling results, there are leakage and venting zones in member Mao-2 near the study area, indicating there is a fracture-cave system in the phreatic zone. From the outcrop, a large cave with a height of 6~10 m has developed about 20~30 m from the top of member Mao-2; From the drilling in the study area, the dolomite of member Mao-2 in the Hechuan area is stably distributed in the middle and lower part of member Mao-2, but the thickness changes greatly (in the range of 2~22 m), which is similar to the cave distribution characteristics in horizontal phreatic zone in a karst system. To sum up, the dolomite in member Mao-2 is controlled by syngenetic karstification which is known for karst features, including caves, that form within a soft, porous, soluble sediment at the same time as it is being cemented into a rock. Speleogenesis and lithogenesis are concurrent [41], and there is a fracture-cave system in the phreatic zone.

Early deposition of the Maokou Formation in the Hechuan area was in the inner gentle ramp of the carbonate ramp, controlled by a NW trending strike-slip fault within the carbonate platform; a localized formation of alternating uplifted and depression paleogeomorphological patterns was established and maintained until member Mao-2 [14,16]. In this geological setting, the bioclastic banks developed in the highlands of paleogeomorphology, and in the highstand stage, the sea level dropped; the beach would emerge from the water surface for a long time, and be leached by meteoric water, forming a syngenetic karstification fracture-cave system. At the same time, the local topography of uplift and depression also makes the local formation of a relatively limited water environment. In this environment, the evaporation of seawater is relatively strong, the salinity of seawater is increased, and the content of Mg^{2+} is also relatively increased. During the transgression period, due to wave action, seabed bioclastics and soft sediment will fill the fractures and caves; with the gradual rise of sea level, it also leads to the continuous replenishment of normal sea water, so that Mg^{2+} is supplemented, and when the sea level is relatively reduced, it will be subject to evaporation, the content of Mg^{2+} in sea water will be increased

(Figure 10). In the shallow burial stage, the particles and marl filled in the fractures and vugs have rapid dolomitization with Mg^{2+} rich seawater. This explains the clear boundary between dolomites and limestone, the absence of dolomitization in limestone "breccia" in dolomites, and the occurrence of dolomitization in limestone only in the fracture (Figure 3).

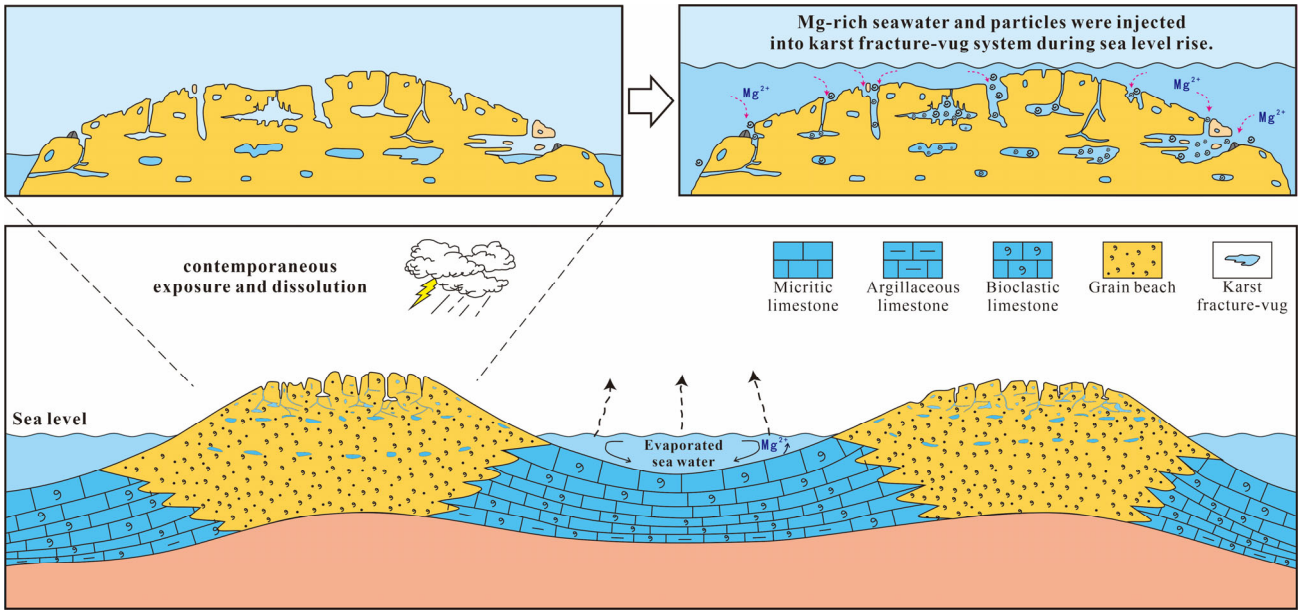

Figure 10. Dolomitization model of the Maokou Formation in Hechuan area.

6.2. Reservoir Main Control Factors

The pore types of the dolomite reservoir in the study area are dominated by heterogeneous vugs and fractures, and locally homogeneous intercrystalline (dissolution) pores are developed. Therefore, it is of great significance to identify the genesis of fractures and vugs for the understanding of reservoir-controlling factors.

According to the tectonic setting of the Sichuan Basin, in the late Middle Permian, Emei taphrogenesis led to the revival of the basement fault in the basin [14], and was subjected to NW stretching, resulting in a large number of syndepositional faults [42]. At this point, tectonic faulting was active in the Hechuan area, and a number of NW trending syndepositional faults were formed; because of the brittleness of dolomite, it is easier to form fractures in dolomite than limestone, so the fractures in the Hechuan area are mainly in the dolomite. As mentioned above, the age of the dolomite in member Mao-2 is 261.0~262.0 Ma, the age of the saddle dolomite in the fractures is 256.0~260.0 Ma; according to the characteristic that the fractures are mainly developed in the dolomite in member Mao-2, it is clear that these fractures were formed after the dolomitization and before the saddle dolomite was filled, which further reveals that the fractures in the dolomite in member Mao-2 are mainly controlled by syndepositional faults. Fractures are not only an important reservoir space, but also a channel for fluid migration in subsequent diagenetic processes.

According to the core characteristics (Figure 4), the vugs in the dolomite of member Mao-2 are mostly developed along the fractures, with the characteristics of non-fabric selectivity and heterogeneous distribution, which shows that these vugs are not controlled by sedimentary facies, but closely related to fractures; after the formation of the dolomite, they underwent modifications due to fluid dissolution along fractures. The Emeishan large igneous province (ELIP) began to erupt around 260 Ma, and the main eruption period was about 259 to 257 Ma [43]. The eruption center is located in the southwest outside the Sichuan Basin, which gradually weakens from west to east, and forms an unusually high heat flow field with a large regional scale [44,45]. The central Sichuan region is in a weakened zone of plume activity in the ELIP, unaffected directly by magma activity, with

minimal melt from mantle plumes; However, it is affected by high heat flow by extension of deep mantle plume materials. In the outer regions of the eruption area, the Mg^{2+} rich strata on the basin floor are driven by an ancient thermal flow, migrating along fractures and developing vugs [8,43,46,47]. In addition, the results of rare earth elements in the dolomite of member Mao-2 at the study area show that there are local Eu anomalies in the dolomite, and element mapping results show significant differences between the host rock and its elements; the host rock edge shows similarity to the elements of the phase I saddle dolomite cement. Therefore, it can be inferred that the host rock has been eroded by hydrothermal fluids, forming an erosion, which subsequently led to the annular-shaped saddle dolomite cement through continuous precipitation. To sum up, it shows that partial dolomite in the study area has been transformed by hydrothermal solution, and the formation of vugs and fractures is related to hydrothermal solution.

Vugs and fractures in the dolomite of member Mao-2 are filled with multi-phase minerals. According to the core observation, saddle dolomite, asphalt, quartz/fluorite and calcite can be identified in turn from the edge of fractures to the center, but not all fractures have a complete filling sequence; some are only filled with one or more of them (Figure 4j,k). According to the results of elemental mapping, it can also be seen that saddle dolomite and quartz fill the vugs in turn, indicating that the pores have been transformed by fluids in different periods. According to the results of previous studies, the Middle–Late Triassic in the study area was the early stage of crude oil cracking, forming an ancient oil reservoir, and the middle stage of the late Jurassic to Middle Cretaceous was the stage of crude oil cracking [48], so it can be inferred that the formation time of asphalt was the early–middle Cretaceous. According to the burial history of central Sichuan Basin [8], in the Late Cretaceous, due to the uplift of the Qinghai–Tibet Plateau and the southeast compression, some early faults in central Sichuan were activated, which led to the similar migration of deep silicon-rich and fluorine-rich hydrothermal solutions along the faults, and to their precipitation into hydrothermal minerals such as quartz and fluorite in the vugs [41], so it can be inferred that quartz/fluorite in the vugs of dolomite in member Mao-2 was formed in the deep burial stage of the late Yanshanian. The Hercynian fault activity once again entered the high-incidence period, and the multi-stage faults activity caused the early strike-slip fault activation. Based on this, it is inferred that the calcite that finally filled in the vugs of member Mao-2 was formed in this period.

Based on this analysis of the origin, pore formation and evolution of dolomite in member Mao-2 of the Maokou Formation the in Hechuan area, and combined with the geological background, the diagenetic sequence and pore evolution curve (Figure 11) of each important stage of the Maokou Formation in the study area are established. Referring to Clyde H. Moore [49], the initial porosity value and the distribution area of residual pores and cement under the microscope were accumulated, and the initial porosity was selected as 30%. After a different diagenesis, the appropriate increase or decrease value was selected to indicate the evolution of porosity. The early diagenetic stage mainly experienced the micritization of sediment mud in the mixed environment of seawater, seawater cementation, the dissolution of meteoric water (forming fracture-cave systems), the collapse of fracture-caves, karst sedimentary filling and dolomitization. The early burial stage mainly experienced mechanical compaction, tectonic fracturing I, hydrothermal dissolution and saddle dolomite cementation. The middle diagenetic stage mainly experienced burial recrystallization and oil-gas charging. In the late diagenetic stage, it mainly experienced tectonic fracturing II, quartz/fluorite filling, tectonic fracturing III and calcite cementation. Among all the main diageneses, syngenetic karstification, dolomitization, tectonic fracture I and hydrothermal dissolution are the most important constructive diageneses, in which syngenetic karstification controls the development of a large fracture-cave system in the subsurface zone, which lays the foundation for subsequent dolomitization. The pre-existing pores are inherited and preserved by penecontemporaneous dolomitization, and the brittle characteristics of dolomite create conditions for a large number of fractures to develop in the later period. The tectonic fracturing I has control of the reservoir, which is not only

an important reservoir space, but also a channel for fluid migration, providing conditions for the formation of vugs. The reservoir has undergone multi-phase hydrothermal transformation, and the early hydrothermal dissolution related to Emei taphrogenesis is the key to the development of dolomite reservoir in member Mao-2, and the porous reservoir is heterogeneous.

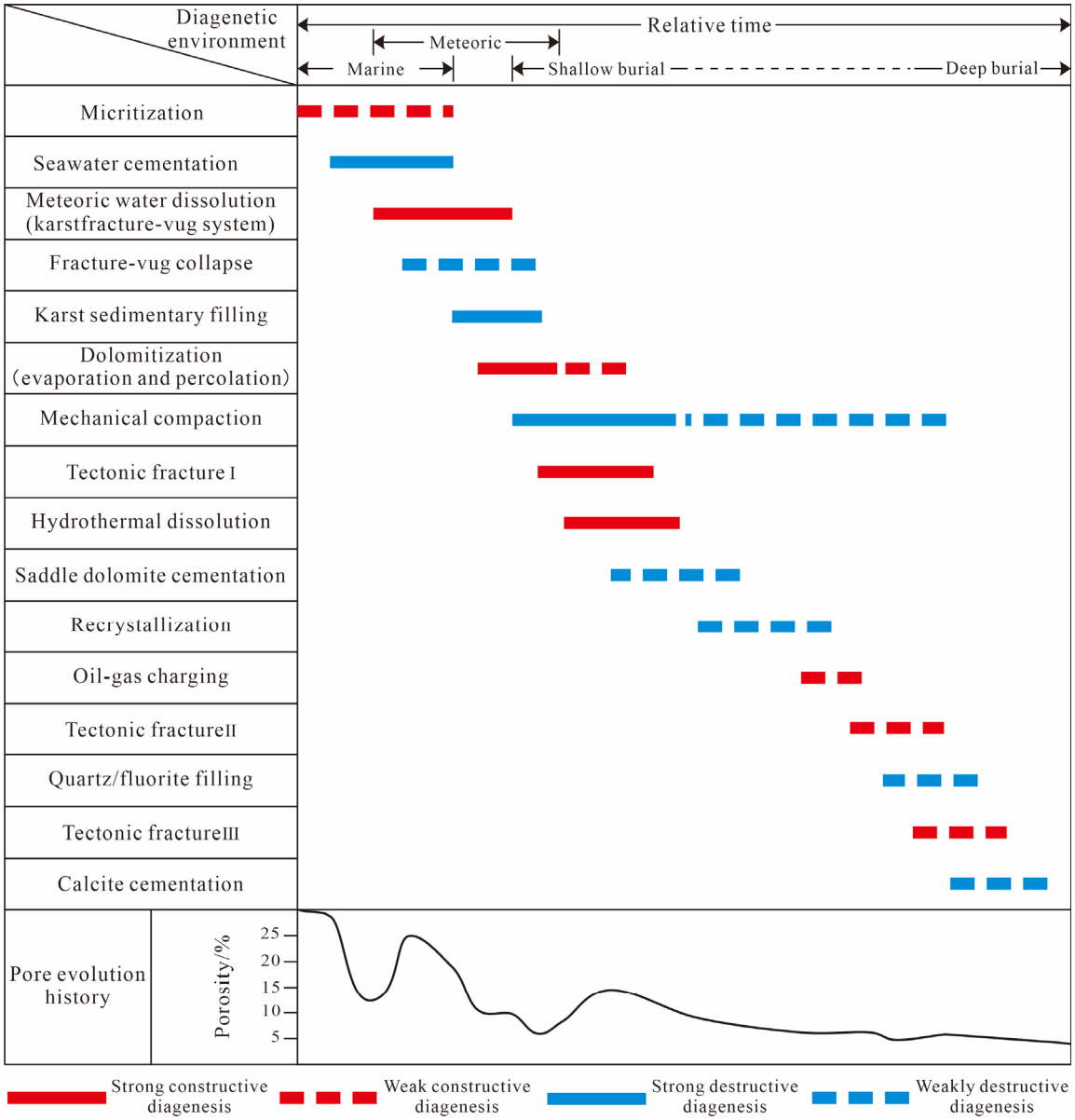

Figure 11. Diagenetic sequence of Maokou Formation.

To sum up, syngenetic karstification, early dolomitization and hydrothermal dissolution related to faults are the main controlling factors for the development of dolomite reservoirs in member Mao-2 of the Hechuan area. Syndepositional faults play a crucial role in the development of dolomite reservoirs. The development of faults not only provides migration channels for hydrothermal fluids, but also serves as an important reservoir space. Syndepositional faults control the distribution law of high-quality reservoirs to a certain extent, playing an important role in the generation, migration, accumulation and accumulation of oil and gas. Accordingly, the prediction of dolomite reservoir development in this study can be achieved by incorporating highlands of paleogeomorphology with syndepositiona faults, which provides a reliable basis for exploration strategies of the Maokou Formation in the Hechuan region.

7. Conclusions

Crystalline dolomite is the main carrier of the reservoir in member Mao-2 in the Hechuan area of Sichuan Basin, and the heterogeneous vugs and fractures are the main reservoir space. The dolomite in member Mao-2 has been characterized by a low degree of cation ordering value (avg. 0.59), with values of $\delta^{13}C$ (avg. 3.87‰), $\delta^{18}O$ (avg. −7.15‰) and $^{87}Sr/^{86}Sr$ (avg. 0.707474); the rare earth elements (REEs) normalized distribution patterns have no obvious outliers, the age determined by laser ablation U-Pb dating range from 261.0 to 262.0 Ma.

Member Mao-2 is controlled by syngenetic karstification to form a large fracture-cave system. The sediment within the fracture-cave system underwent dolomitization during the penecontemporaneous period with local seawater as the dolomitization fluid.

The fracture-cave system formed under control of syngenetic karstification laid the foundations for subsequent dolomitization. Penecontemporaneous dolomitization inherits and preserves the pre-existing pores, and the brittle characteristics of dolomite played a pivotal role in the extensive development of later-stage fractures. The NW trending faults associated with Emei taphrogenesis have a significant control over the reservoir, serving as important reservoir spaces and fluid migration pathways. Reservoirs have undergone multi-phase hydrothermal transformation, most of the vugs exit along the fractures in a heterogeneous way, so the highlands of paleogeomorphology with syndepositional faults are favorable areas for dolomite reservoirs.

Author Contributions: Conceptualization, J.Z. and X.B.; methodology, J.Z. and K.D.; software, K.D. and J.D.; validation, J.Z. and X.B.; formal analysis, S.H. and Y.L.; investigation, J.Z. and K.D.; resources, X.B. and S.H.; data curation, J.D. and Y.L.; writing—original draft preparation, J.Z. and K.D.; writing—review and editing, J.Z.; visualization, K.D. and J.D.; supervision, J.Z.; project administration, J.Z. and X.B.; funding acquisition, J.Z. and X.B. All authors have read and agreed to the published version of the manuscript.

Funding: This research was funded by the Scientific Research and Technology Development Project of PetroChina Company Limited (Grant No. 2021DJ0501).

Data Availability Statement: Data are available upon reasonable request. The data that support the findings of this study are available on request from the corresponding author. The data are not publicly available due to privacy or ethical restrictions.

Acknowledgments: We would thank Anjiang Shen and Jingao Zhou for their valuable suggestions, Xianying Luo and Feng Liang for their guidance in the experiments. We would also like to thank Mao Zhu, Yi Hao, Qianying Yao and Kedan Zhu for the help in data collection.

Conflicts of Interest: The authors declare no conflict of interest.

References

1. Ma, Y.S.; Guo, X.S.; Guo, T.L.; Huang, R.; Cai, X.; Li, G.X. The Puguang gas field: New giant discovery in the mature Sichuan Basin, southwest China. *AAPG Bull.* **2007**, *91*, 627–643. [CrossRef]
2. Guo, X.S.; HU, D.F.; Li, Y.P.; Duan, J.B.; Ji, C.H.; Duan, H. Discovery and theoretical and technical innovations of Yuanba gas field in Sichuan Basin, SW China. *Pet. Explor. Dev.* **2018**, *45*, 14–26. [CrossRef]
3. Du, J.H.; Zhou, C.N.; Xu, C.C.; He, H.Q.; Shen, P.; Yang, Y.M.; Li, Y.L.; Wei, G.Q.; Wang, Z.C.; Yang, Y. Theoretical and technical innovations in strategic discovery of a giant gas field in Cambrian Longwangmiao Formation of central Sichuan paleo-uplift, Sichuan Basin. *Pet. Explor. Dev.* **2014**, *41*, 268–277. [CrossRef]
4. Yang, Y.M.; Yang, Y.; Wen, L.; Zhang, X.H.; Chen, C.; Chen, K.; Zhang, Y.; Di, G.L.; Wang, H.; Xie, C. New progress and prospect of Permian natural gas exploration in Sichuan Basin. *Nat. Gas Ind.* **2020**, *40*, 10–22. [CrossRef]
5. Yang, Y.; Xie, J.R.; Zhao, L.Z.; Huang, P.H.; Zhang, X.H.; Chen, C.; Zhang, B.J.; Wen, L.; Wang, H.; Gao, Z.L.; et al. Breakthrough of natural gas exploration in the beach facies porous dolomite reservoir of Middle Permian Maokou Formation in the Sichuan Basin and its implications: A case study of the tridimensional exploration of Well JT1 in the central-northern Sichuan Basin. *Nat. Gas Ind.* **2021**, *41*, 1–9. [CrossRef]
6. Liu, H.; Ma, T.; Tan, X.C.; Zeng, W.; Hu, G.; Xiao, D.; Luo, B.; Shan, S.J.; Su, C.P. Origin of structurally controlled hydrothermal dolomite in epigenetic karst system during shallow burial: An example from Middle Permian Maokou Formation, central Sichuan Basin, SW China. *Pet. Explor. Dev.* **2016**, *43*, 916–927. [CrossRef]

7. Jiang, Y.Q.; Gu, Y.F.; Li, K.H.; Li, S.; Luo, M.S.; He, B. Spatial types and genesis of Middle Permian hydrothermal dolomite reservoirs in central Sichuan Basin. *Nat. Gas Ind.* **2018**, *38*, 16–24. [CrossRef]
8. Liu, J.Q.; Zheng, H.F.; Liu, B.; Liu, H.G.; Shi, K.B.; Guo, R.T.; Zhang, X.F. Characteristics and genetic mechanism of the dolomite in the Middle Permian Maokou Formation, central Sichuan area. *Acta Pet. Sin.* **2017**, *38*, 386–398. [CrossRef]
9. Hu, A.P.; Pan, L.Y.; Hao, Y.; Shen, A.J.; Gu, M.F. Origin, Characteristics and Distribution of Dolostone Reservoir in Qixia Formation and Maokou Formation, Sichuan Basin, China. *Marin. Orig. Petrl. Geol.* **2018**, *23*, 39–52. [CrossRef]
10. Hu, D.F.; Wang, L.J.; Huang, R.C.; Duan, J.B.; Xu, Z.X.; Pan, L. Characteristics of dolomite reservoirs in the middle Permian Maokou Formation in the eastern Sichuan Basin and their main controlling factors. *Nat. Gas Ind.* **2019**, *39*, 13–21. [CrossRef]
11. Li, R.B.; Duan, J.B.; Pan, L.; Li, H. Genetic mechanism and main controlling factors of the Middle Permian Maokou Formation dolomite reservoirs in the eastern Sichuan Basin. *Nat. Gas Geosci.* **2021**, *32*, 1347–1357. [CrossRef]
12. Zhao, W.Z.; Shen, A.J.; Hu, S.Y.; Zhang, B.M.; Pan, W.Q.; Zhou, J.G.; Wang, Z.C. Geological conditions and distributional features of large-scale carbonate reservoirs onshore China. *Pet. Explor. Dev.* **2012**, *39*, 1–12. [CrossRef]
13. Liu, S.G.; Yang, Y.; Deng, B.; Zhong, Y.; Wen, L.; Sun, W.; Li, Z.W.; Jansa, L.; Li, J.X.; Song, J.M.; et al. Tectonic evolution of the Sichuan Basin, Southwest China. *Earth-Sci. Rev.* **2021**, *213*, 103470. [CrossRef]
14. Ma, B.S.; Liang, H.; Wu, G.H.; Tang, Q.S.; Tian, W.Z.; Zhang, C.; Yang, S.; Zhong, Y.; Zhang, X.; Zhang, Z.L. Formation and evolution of the strike-slip faults in the central Sichuan Basin, SW China. *Pet. Explor. Dev.* **2023**, *50*, 333–345. [CrossRef]
15. Gu, M.F.; Liu, R.; Zhang, H.; He, Y.; Li, K.Y.; Hao, Y.; Jiang, H.; Li, W.Z. Characteristics of Caledonian tectonic movement and its geological response in Sichuan Basin. *Nat. Gas Ind.* **2023**, *43*, 32–43.
16. Zhong, Y.; Yang, Y.M.; Wen, L.; Luo, B.; Xiao, D.; Tan, X.C.; Zhao, L.K.; Li, M.L. Sedimentary environments controlled by tectonics and induced differential subsidence: A perspective in the Permian Liangshan and Qixia Formations, northwestern Sichuan Basin, China. *J. Cent. South Univ.* **2020**, *27*, 3398–3416. [CrossRef]
17. Huang, S.P.; Jiang, Q.C.; Jiang, H.; Tang, Q.S.; Zeng, F.Y.; Lu, W.H.; Hao, C.G.; Yuan, M.; Wu, Y. Genetic and source differences of gases in the Middle Permian Qixia and Maokou formations in the Sichuan Basin, SW China. *Org. Geochem.* **2023**, *178*, 104574. [CrossRef]
18. Zhao, Z.J.; Zhou, H.; Chen, X.; Liu, Y.H.; Zhang, Y.B.; Liu, Y.E.; Yang, Y. Sequence lithofacies paleogeography and favorable exploration zones of the Permian in Sichuan Basin and adjacent areas, China. *Acta Pet. Sin.* **2012**, *33*, 35–51. [CrossRef]
19. Li, D.J.; Chen, H.; Chen, H.D.; Liang, H.; Peng, C.; Xia, M.; Duan, H.Z. Relationship between reservoir development in the Middle Permian Maokou Formation and paleostructure evolution in the Sichuan Basin. *Oil Gas Geol.* **2016**, *37*, 756–763. [CrossRef]
20. Hu, M.Y.; Hu, Z.G.; Wei, G.Q.; Yang, W.; Liu, M.C. Sequence lithofacies paleogeography and reservoir potential of the Maokou Formation in Sichuan Basin. *Pet. Explor. Dev.* **2012**, *39*, 45–55. [CrossRef]
21. Tian, X.B.; Shi, J.B.; Dong, J.H.; Tan, W.C.; Yin, C.H.; Li, Q.; Song, Z.Y.; Zhang, K.; Xiao, C.T. New understanding of sedimentary facies of the first member of Maokou Formation based on the latest drilling in central Sichuan Basin. *Nat. Gas Geosci.* **2021**, *32*, 1646–1655.
22. Goldsmith, J.R.; Graf, D.L. Structural and compositional variations in some natural dolomites. *J. Geol.* **1958**, *66*, 678–693. [CrossRef]
23. Helie, J.F.; Adamowicz-Walczak, A.; Middlestead, P.; Chartrand, M.M.G.; Mester, Z.; Meija, J. Discontinuity in the Realization of the Vienna Peedee Belemnite Carbon Isotope Ratio Scale. *Anal. Chem.* **2021**, *93*, 10740–10743. [CrossRef]
24. Shen, A.J.; Zhao, W.Z.; Hu, A.P.; Wang, H.; Liang, F.; Wang, Y.S. The datingand temperature measurement technologies for carbonate minerals and their application in hydrocarbon accumulation research in the paleo-uplift in central Sichuan Basin, SW China. *Pet. Explor. Dev.* **2021**, *48*, 476–487. [CrossRef]
25. Merlini, M.; Sapelli, F. High-temperature and high-pressure behavior of carbonates in the ternary diagram $CaCO_3$-$MgCO_3$-$FeCO_3$. *Am. Mineral.* **2006**, *101*, 1423–1430. [CrossRef]
26. Deng, M.; Qian, G.R.; Tang, M.S. Ordered index and dedolomitization of dolomite crystals. *J. Nanjing Univ. Chem. Technol.* **2001**, *23*, 1–5. [CrossRef]
27. Zheng, J.F.; Wang, H.; Shen, A.J.; Luo, X.Y.; Zhao, C.; Dai, K. Genesis of Dolomite Reservoir in Ediacaran Chigbrak Formation of Tarim Basin, NW China: Evidence from U–Pb Dating, Isotope and Element Geochemistry. *Am. Mineral.* **2023**, *13*, 725. [CrossRef]
28. Northrop, D.A.; Clayton, R.N. Oxygen-isotope fractionations in systems containing dolomite. *J. Geol.* **1966**, *74*, 174–196. [CrossRef]
29. Saller, A.H.; Dickson, J.A.D. Partial dolomitization of a Pennsylvanian limestone buildup by hydrothermal fluids and its effect on reservoir quality and performance. *AAPG Bull.* **2011**, *95*, 1745–1762. [CrossRef]
30. Veizer, J.; Ala, D.; Azmy, K.; Bruckschen, P.; Buhl, D.; Bruhn, F.; Carden, G.A.; Diener, A.; Ebneth, S.; Godderis, Y. 87Sr/86Sr, δ13C and δ18O evolution of Phanerozoic seawater. *Chem. Geol.* **1999**, *161*, 59–88. [CrossRef]
31. Baud, A.; Magaritz, M.; Holser, W.T. Permian-Triassic of the Tethys: Carbon isotope studies. *Geol. Rundsch.* **1989**, *78*, 649–677. [CrossRef]
32. Burns, S.J.; Haudenschild, U.; Matter, A. The strontium isotopic composition of carbonates from the late Precambrian (∼560–540 Ma) Huqf Group of Oman. *Chem. Geol.* **1994**, *111*, 269–282. [CrossRef]
33. Lottermoser, B.G. Rare earth elements and hydrothermal ore formation processes. *Ore Geol. Rev.* **1992**, *7*, 25–41. [CrossRef]
34. Zheng, J.F.; Shen, A.J.; Qiao, Z.F.; Wu, X.N.; Zhang, T.F. Characteristics and pore genesis of dolomite in the Penglaiba Formation in Keping-Bachu outcrop area. *Acta Pet. Sin.* **2014**, *35*, 664–672. [CrossRef]
35. McLennan, S.M.; Taylor, S.; McGregor, V. Geochemistry of Archean metasedimentary rocks from West Greenland. *Geochim. Cosmochim. Acta* **1984**, *48*, 1–13. [CrossRef]

36. Drost, K.; Chew, D.; Petrus, J.A.; Scholze, F.; Woodhead, J.D.; Schneider, J.W.; Harper, D.A.T. An Image Mapping Approach to U-Pb LA-ICP-MS Carbonate Dating and Applications to Direct Dating of Carbonate Sedimentation. *Geochem. Geophys. Geosyst.* **2018**, *19*, 4631–4648. [CrossRef]
37. Zheng, J.; Zhu, Y.J.; Huang, L.L.; Guo, Y.; Hu, F.J. Geochemical Characteristics and Their Geological Significance of Lower Cambrian Xiaoerblak Formation in Northwestern Tarim Basin, China. *Am. Minerals.* **2022**, *12*, 781. [CrossRef]
38. Shen, A.J.; Luo, X.Y.; Hu, A.P.; Qiao, Z.F.; Zhang, J. Dolomitization evolution and its effects on hydrocarbon reservoir formation from penecontemporaneous to deep burial environment. *Pet. Explor. Dev.* **2022**, *49*, 637–647. [CrossRef]
39. Korte, C.; Jasper, T.; Kozur, H.W.; Veizer, J. δ18O and δ13C of Permian brachiopods: A record of seawater evolution and continental glaciation. *Palaeogeogr. Palaeoclimatol. Palaeoecol.* **2005**, *224*, 333–351. [CrossRef]
40. Zheng, J.F.; Huang, L.L.; Yuan, W.F.; Zhu, Y.J.; Qiao, Z.F. Geochemical features and its significance of sedimentary and diagenetic environment in the Lower Cambrian Xiaoerblak Formation of Keping area, Tarim Basin. *Nat. Gas Geosci.* **2020**, *31*, 698–709. [CrossRef]
41. Zheng, J.F.; Shen, A.J.; Liu, Y.F.; Chen, Y.Q. Multi-parameter comprehensive identification of the genesis of Lower Paleozoic dolomite in Tarim Basin, China. *Acta Pet. Sin.* **2012**, *33*, 145–153. [CrossRef]
42. Grimes, K. Syngenetic Karst in Australia: A Review. *Helictite* **2003**, *39*, 27–38.
43. Fu, X.D.; Zhang, B.J.; Wang, Z.C.; Lei, M.; Zhang, J.Y.; Guang, S.W.; Li, W.Z.; Zhong, Y.; Gu, M.F.; Chen, T. Strike-Slip Faults in Central and Western Sichuan Basin and Their Control Functions on Hydrocarbon Accumulation. *Earth Sci.* **2023**, *48*, 2221–2237.
44. Sun, Z.M.; Bian, C.R.; Liu, G.X. Advances on Emeishan Mantle Plume and Discussions on Dynamic Mechanism of Formation of Sichuan Basin in Permian. *Geosciences* **2023**, 1–15. [CrossRef]
45. Liang, X.Y.; Li, H.; Zhang, D.D.; Yang, K.; Zhou, D.W.; Zheng, T.Y.; Dong, Y.K.; Zhai, L.G. Geochemical characteristics and genetic analysis of Huayingshan Emeishan basalt in Sichuan Basin. *Sci. Geol. Sin.* **2022**, *56*, 288–302. [CrossRef]
46. Zhu, C.Q.; Xu, M.; Yuan, Y.S.; Zhao, Y.Q.; Shan, J.N.; He, Z.G.; Tian, Y.T.; Hu, S.B. Palaeo-geothermal response and record of the effusing of Emeishan basalts in Sichuan basin. *Chin. Sci. Bull.* **2010**, *55*, 474–482. [CrossRef]
47. Li, H.B.; Zhang, Z.C.; Lv, L.S.; Wang, Y.F.; Kou, C.H.; Li, Y.S.; Liao, B.L. Isopach maps of the Qixia and Maokou formations: Implication for mantle plume model of the Emeishan large igneous province. *Acta Pet. Sin.* **2011**, *27*, 2963–2974.
48. He, W.Y.; Meng, Q.A.; Yin, C.H.; Wang, X.D.; Zhang, H.J.; Shi, J.B. Geological characteristics and favorable exploration plays of gas in Qixia Formation dolomite in Hechuan-Tongnan area of Sichuan Basin. *Petroleum Pet. Geol. Oilfield Dev. Daqing.* **2022**, *41*, 1–11. [CrossRef]
49. Clyde, H.M. Carbonate reservoirs-porosity evolution and diagenesis in a sequence stratigraphic framework. *Mar. Pet. Geol.* **2001**, *19*, 293–298. [CrossRef]